International Journal for Multiscale Computational Engineering, 2(2)313-327(2004)

Coarse-Grained Kinetic Monte Carlo Simulation of Copper Electrodeposition with Additives

*Timothy O. Drews, Richard D. Braatz, & Richard C. Alkire**

Department of Chemical and Biomolecular Engineering
University of Illinois at Urbana-Champaign, Urbana, IL 61801

ABSTRACT

A (2+1)D kinetic Monte Carlo (KMC) code was developed for coarse-grained as well as atomic-scale simulations that require detailed consideration of complex surface-reaction mechanisms associated with electrodeposition of copper in the presence of additives. The physical system chosen for simulation is similar to that used by the microelectronics industry to fabricate on-chip interconnects, where additives are used to tailor shape evolution. Although economically significant, such systems are often designed in an empirical manner that would be greatly enhanced by improved understanding of the additive mechanism gained through simulations. By comparing simulated results at atomic as well as coarse-grained scales with theoretical results obtained analytically for various limiting cases of behavior, the validity of the KMC code was tested. It was found that the surface roughness at a specified length scale can be accurately simulated by using a coarse-grained KMC code with lattice spacing of 1/10 or smaller than that of the specified length scale—a result that is particularly useful for comparing experimental data on surface roughness with numerical simulations. For second-order homogeneous surface reactions, it is shown that the KMC-simulated surface coverage approaches the analytical surface coverage as surface mixing is increased by increasing the surface diffusion rate. The results verified the numerical accuracy and the reduced computational cost of the coarse-grained KMC approach for simulating complex chemical and electrochemical mechanisms.

* Address all correspondence to Richard C. Alkire, University of Illinois at Urbana-Champaign, 600 S. Mathews Ave., Box C-3, MC 712, Urbana, IL 61801, r-alkire@uiuc.edu

0731-8898/04/$20.00

1. INTRODUCTION

Electrochemical metal deposition processes that use trace amounts of solution additives support a wide range of industrial activities that have significant economic impact. Additives influence mechanistic pathways, as well as form adsorbed molecular stencils that guide surface traffic patterns during the course of lattice formation and shape evolution. Such phenomena determine the course of events at the nanoscale (nucleation and early stages of crystal growth), microscale (surface roughness, net geometric shape), and macroscale (process equipment design). Moreover, the deposit shape represents the integrated signature of a hierarchy of complex multiscale, multiphenomena events, which poses a significant scientific challenge in determining how the deposit shape evolved.

Although a significant level of qualitative intuitive insight about additive mechanisms can be learned through experience, various kinds of uncertainties can nevertheless arise. For example, not only is understanding of the fundamental physical phenomena uncertain, but also how such phenomena exert influence on the macroscopic outcomes, particularly shape evolution. The motivation for the present work is to establish a stochastic method that will serve as a building block suitable for use in multiscale modeling. Traditional quantitative engineering design methods are typically based on a continuum approach, which is not always able to accurately resolve the nanoscale region, where product quality is determined by the action of additives. The particular application described here involves simulating the influence of additives on shape evolution at the near-molecular scale during copper electrodeposition; a key step in processing on-chip interconnects for microelectronic devices.

In the present effort, a coarse-grained kinetic Monte Carlo (KMC) code was developed to simulate the influence of additives on roughness evolution during electrodeposition. In coarse-grained simulations, the user selects the desired scale by defining the size of *mesoparticles,* which represent packets of like atoms or molecules, while also assigning them some of the attributes associated with the behavior of individual atoms/molecules. Coarse-grained simulations thus provide an approximate method for incorporating atomistic physics into mesoscale phenomena. For example, surface diffusion, which at the atomic scale is modeled as single atoms moving among different sites on the surface where the likelihood of possible movements is regulated by the local environment around the atoms, is modeled similarly at the coarse-grained level. Meso-particles thus diffuse along the surface with movements governed by the same physics that apply to single-particle diffusion.

Coarse-grained simulation approaches have recently been used in a variety of fields. A coarse-grained Monte Carlo spin-flip simulation model was developed to simulate the adsorption and desorption of molecules from a surface to and from the gas phase [1] and diffusion of interacting species on a lattice [2]. Coarse-grained Monte Carlo simulations also have been performed to simulate surfactant solutions, particularly surfactant aggregate structure formation, binary and ternary phase diagrams, the nature of equilibrium micelles, and solubilization by micelles [3]. The interactions between globular proteins with differing spatial distributions of hydrophobic surface residues and a slightly hydrophobic polymer were simulated with a coarse-grained Metropolis Monte Carlo model, where the proteins were modeled as hard spheres with discrete interaction sites at the surface and the polymer is modeled as a chain of beads connected by harmonic bonds [4]. Also, biomembranes have been simulated with a coarse-grained model that integrates both Monte Carlo and molecular dynamics techniques and simulates molecules as groups

of spheres, where the spheres are comprised of many atoms [5]. Connections have been made between coarse-grained Monte Carlo algorithms and renormalization group theories [2,6]

We have recently reported simulation studies with a coarse-grained 3D KMC model [7, 8, 9, 10, 11] that used a rate constant based approach to determine the possible actions that a mesoparticle could make at a given Monte Carlo time step. The code used in those publications checked each active mesoparticle at each species' Monte Carlo time step and either attempted an action or selected to do nothing. The improved approach reported below makes more challenging simulations possible, particularly for low additive concentrations in the ppb to ppm range, as well as steric (or proximity) effects. In addition, the KMC code reported below provides the capability for simulating complex heterogeneous mechanisms, such as accomplished recently by Dooling and Broadbent [12], while having the additional features of handling electrochemical reactions and simulating a wider range of length scales through coarse-graining. The simulation results reported here have been performed at both the coarse-grained and atomic scale, and have been compared to analytical solutions of kinetic equations to verify the simulation model.

3. DESCRIPTION OF THE SIMULATION CODE

The coarse-grained KMC code simulates phenomena that take place on the surface of the metal during electrodeposition, including adsorption, desorption, surface diffusion, and surface reactions, as well as proposed chemical reaction mechanisms that incorporate these actions. The size of the coarse-grained mesoparticles was chosen so that deposit roughness evolution could be simulated at the same time- and length-scales that can be observed experimentally (e.g., with atomic force microscopy). The long-term goal is to compare coarse-grained KMC simulation results with comparable experimental data to enable the evaluation of proposed mechanisms of additive behavior.

A (2+1)D formulation was used for the lattice sites consisting of the 2D plane of the surface on which the deposit grows upward during roughness evolution (the +1D component). Lattice sites above or below the surface are not considered. The (2+1)D formulation is also referred to as a solid-on-solid formulation [13, 14, 15]. In a KMC simulation algorithm, the transition probabilities are determined by the rates of the associated processes; the rates of possible actions at each surface site are determined; and an action is performed at one surface site per Monte Carlo time step.

2.1. KMC Algorithm

The algorithm employed in the (2+1)D KMC code can be described as follows. In each system there are N species that can possibly undergo k transition events [16]. Each of the k transition events have a rate, R_i, associated with them. The N species are then partitioned over the possible transition events. Once the rates of the events are calculated, a list of transition probabilities can be constructed in terms of the rates in such a way that there is a dynamical hierarchy established between the rates. The dynamical hierarchy is established by the individual transition probabilities

$$W_i = \frac{R_i}{\xi_{\max}}, \tag{1}$$

where $\xi_{\max} \geq \sum_i R_i$. Real time is simulated by using the time increment

$$\tau_i = \frac{1}{\sum_i n_i r_i}, \tag{2}$$

where n_i is the number of species out of N that are capable of undergoing a transition event with a rate r_i [17, 18].

The KMC algorithm employed here is similar to that described by Levi and Kotrla [19] and Battaile *et al*. [20] used for simulations of crystal growth:

1. Choose a random number r from a uniform distribution in the range (0,1).
2. Select the transition event from the list by selecting the first index s for which $\sum_{i=1}^{s} R_i \geq r$.
3. Proceed with R_s.
4. Update all R_i that have changed as a result of making the move.
5. Advance the time in the simulations by τ_i.

The rates are binned by type in order to speed up the simulations. Each time a rate is selected, an instance of that rate is executed. The instance of the rate is selected based on the same random number that was generated to select which rate is executed. The algorithm is coded by using structured lists to minimize the computational expense:

1. Information about each rate is stored in a matrix. The site number is unique for each site on the surface. Periodic boundary conditions are used in the x and y directions.
2. At the beginning of the simulation, all of the rates for all possible moves are tabulated and cataloged. These rates are only recalculated when a move occurs at a site or one of its eight nearest neighbors.
3. All of the possible rates in the system are binned to create a list that is used to select what events occur.
4. The rates are normalized and a random number is generated on the interval (0,1).
5. Once the random number is generated, the appropriate event is selected from the list.
6. Next an instance of that event is selected from the bin for that rate and the action is executed.
7. The appropriate neighbor rates are updated in the site list depending on the action that is taken.
8. The time in the system is updated and the process is repeated.

The (2+1)D KMC model presented here uses the rate-based approach that formulates all actions in terms of rates and checks a single site per Monte Carlo time step. Null events are eliminated in this approach. There is a single Monte Carlo time step in the simulations that is a function of the species and their associated rates. It is possible to simulate the effect of low-concentration additives and steric effects with this KMC formulation.

All simulations presented in this work were run on the IBM P690 at the National Center for Supercomputing Applications (NCSA). Each simulation was run on a single processor. The simulations typically required less than 5 min to complete, but could take several hours to complete for high surface diffusion rate constants.

2.2. The Mesoparticle Approach

Each mesoparticle [21, 22, 23] in the coarse-grained mode of the (2+1)D KMC simulation code consists of a group of molecules at the same vertical position. However, the effect of monolayers is important with many additive systems with the result that mesoparticles that are more than one-molecule high may not capture some important effects, such as surface blocking, because the entire monolayer could be contained in a single mesoparticle due to the partitioning employed. Verification simulations

for the mesoparticle approach are provided in Sections 3 and 4.

2.3. KMC Code Performance

An adsorption simulation is used to illustrate the performance of the KMC simulation code for varying amounts of coarse-graining (see Section 3.1 for details on implementation). In the simulations, copper is allowed to adsorb onto a 5 μm × 5 μm surface and the simulations are performed with 0.5 M Cu^{2+} at an applied overpotential of -0.10 V. Five different lattices were simulated: 32 × 32, 64 × 64, 128 × 128, 256 × 256, and 512 × 512.

Figure 1 represents a plot of the time required for the simulation versus the number of lattice sites in the simulation. It may be seen that the simulation time increases superlinearly with the number of lattice sites. The change in slope between 10^3 and 10^4 lattice sites occurred because, for a small number of lattice sites, the simulation time was dominated by the time to write data to files. It may be seen, not surprisingly, that the reduction in computational cost from coarse-graining can be many orders of magnitude. In Fig. 2, the mass of copper deposited according to the KMC simulations is plotted as a function of the number of lattice sites simulated. Except for the 32 × 32 lattice, the simulated amount deviated from the theoretical amount of deposited copper by less than 1%.

3. VERIFICATION SIMULATIONS

Several different sets of verification simulations were performed to compare the coarse-grained KMC simulations with theoretical results. Validating the KMC model in this manner will facilitate the comparison of the KMC simulations and experimental data because the fidelity of the KMC model will be known. In this section, the coarse-grained implementations of adsorption, surface reactions, and surface diffusion are evaluated.

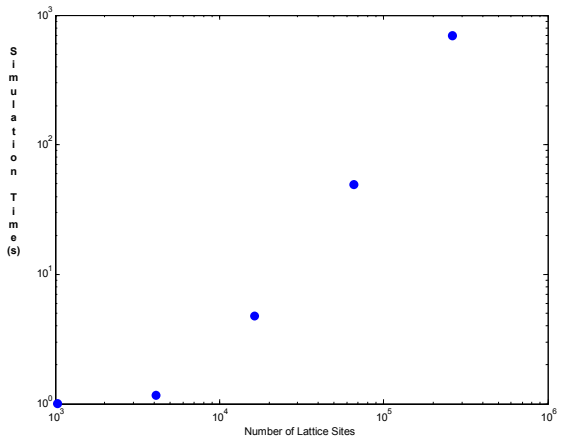

FIGURE 1. Time required for a 1 s simulation of adsorption of copper from solution onto the substrate. The adsorption simulations are performed on a 5 μm × 5 μm patch, with varying discretization of the simulation domain. Simulations were performed with 0.5 M Cu^{2+} at an applied overpotential of -0.10 V.

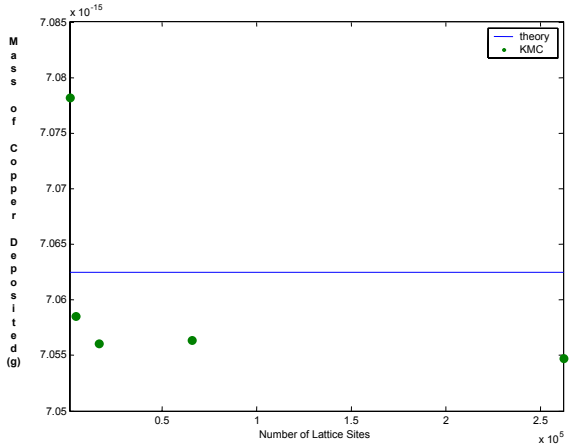

FIGURE 2. Mass of copper deposited during a 1 s simulation of adsorption of copper from solution onto the substrate. The adsorption simulations are performed on a 5 μm × 5 μm patch, with varying discretization of the simulation domain. For all cases, the amount of copper deposited in the KMC simulations deviated from the theoretical amount of copper that should be deposited by less than 1%. Simulations were performed with 0.5 M Cu^{2+} at an applied overpotential of -0.10 V.

3.1. Low-Order Electrochemical Reactions

A common mechanism encountered during electrodeposition consists of an electrochemical adsorption step followed by an electrochemical surface reaction. Consider first the electrochemical adsorption reaction $A(aq) + e^- \rightarrow B(ads)$, in which a B mesoparticle is formed on the surface from an equivalent number of electrons and molecules of A in solution. The rate equation is based on Tafel kinetics [24, 25]

$$\frac{i}{nF} = k\, C_A\big|_{z=0} \left(1-\theta_\beta\right) C'_{total} e^{\left(-\frac{\alpha n F \eta}{RT}\right)} \tag{3}$$

where $\frac{i}{nF}$ is the adsorption rate in units of mol/(m^2-s); i is the current density (A/m^2), n is the number of charge equivalents per mole (eq/mol), F is Faraday's constant, k is the heterogeneous rate constant (m^3/mol-s), θ_β is the sum of the coverage's of all species where A is not permitted to adsorb, C'_{total} is the concentration of surface sites (mol/m^2), and $C_A\big|_{z=0}$ is the concentration of Species A in the bulk at the surface and can be obtained from a continuum code, or, in the case of negligible bulk diffusion limitations to the surface, the concentration can be specified by the user and fixed for the duration of the simulation. If Eq. 3 is rewritten so that n and F are on the right-hand side, the term $nFkC_A\big|_{z=0}$ is the exchange current density j_0, which is readily accessible in many experimental systems [26]

The associated rate in the coarse-grained KMC code, rate$_{MC}$, is the number of events for one site occupied by an A mesoparticle per second. A careful accounting for the size of the mesoparticle and the number of lattice sites gives the equation

$$\text{rate}_{\text{MC}} = k\, C_A\big|_{z=0} e^{\left(-\frac{\alpha n F \eta}{RT}\right)} \tag{4}$$

that is not a function of the lattice spacing, because the larger quantity of molecules that react at each event (compared to an atomic-scale computation) is exactly compensated by the reduced number of lattice sites.

Verification simulations for a range of mesoparticle sizes were reported in Section 2.3. The surface roughness at various times is reported in Fig. 3 for a range of mesoparticle sizes from atomic (0.256 nm) on a 512 × 512 lattice to 16 × atomic on a 32 × 32 lattice. Increasing the mesoparticle size by a factor of N shifts the length at which the surface reaches the saturation roughness (defined as the surface roughness at long length scales) by about the same factor of N (compared to the atomic case). Inspection of Fig. 3 indicates that the surface roughness at a specified length scale can be accurately simulated provided that a coarse-grained KMC code is used whose lattice spacing is 1/10 (or smaller) of that length scale.

Now consider the heterogeneous reaction $A(aq) + B(ads) + 2e^- \rightarrow C(ads) + D(s)$, where A in solution interacts with an adsorbed B mesoparticle on the surface and two electrons. The products are an adsorbed C mesoparticle on top of a D mesoparticle. For a first-order rate equation with the same general form as Eq. (3), the expression for the KMC rate would be similar to Eq. (4). For a surface of B initially covered with a monolayer of A, Figs. 4a and 4b illustrate how the coverage of A obtained from theory compares with KMC simulations for both 10 and 100 nm mesoparticle sizes. It may be seen that the simulated coverage coincides closely with the theoretical coverage for all times investigated here.

3.2. Surface Diffusion

The rate expression for surface diffusion is [27, 28, 29]

$$r = w_i e^{-E_i/RT}, \tag{5}$$

where w_i is the jump frequency (hops/s) and E_i is the energy barrier for surface diffusion, which depends on the local environment of the mesoparticle. In the case of a flat featureless surface, E_i is the energy barrier for movement from one site to another. The mesoparticle can be restricted from diffusing onto certain species and can have different surface-diffusion energy barriers for diffusing on different types of species.

The following derives the jump frequencies in terms of the diffusion coefficient and mesoparticle size for a simple cubic lattice (similar equations for other lattices are derived in a similar manner). Define c_i as the surface concentration at a plane i, and ΔL as the distance between lattice sites. Fick's Law relates the lattice spacing and the diffusion coefficient to the flux between planes 1 and 2:

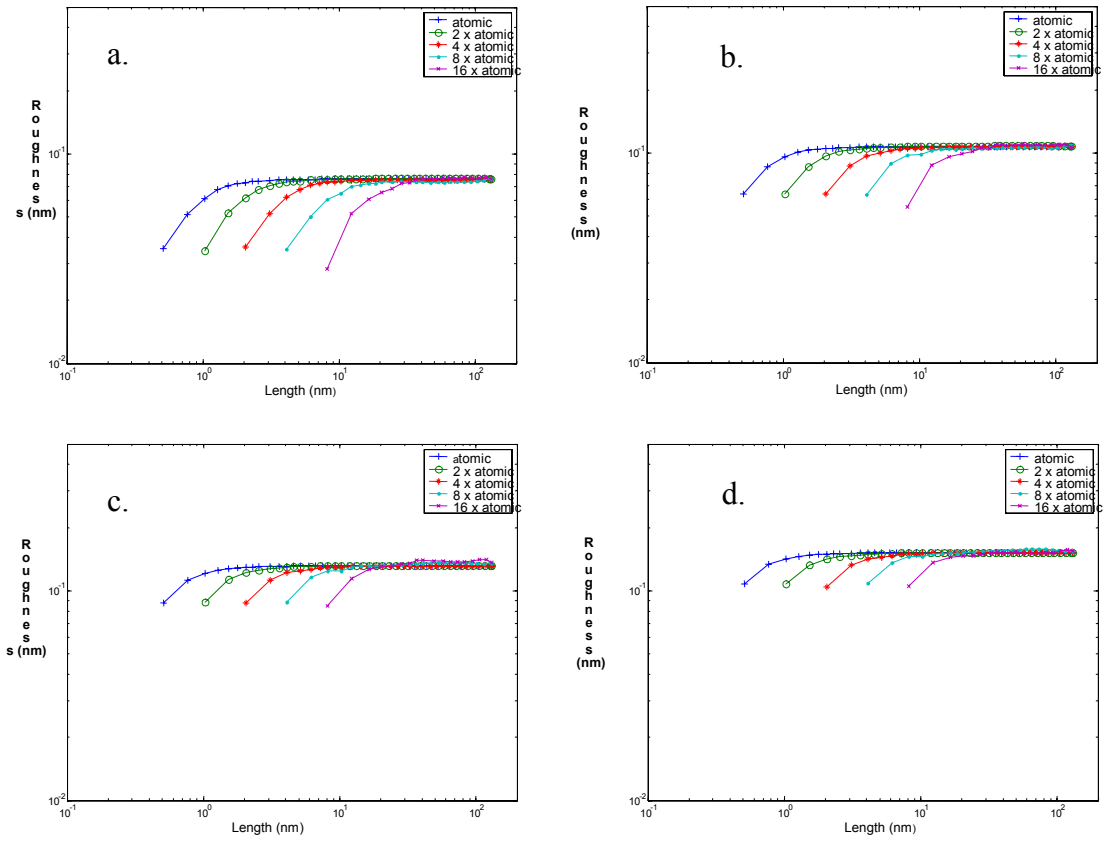

FIGURE 3. Root mean square roughness plotted as a function of the length across the surface. The simulation domain size is held constant at 131.072 nm, with varying discretization for each simulation. Simulation results are after **(a)** 0.5 s, **(b)** 1.0 s, and **(c)** 1.5 s, and **(d)**. 2.0 s.

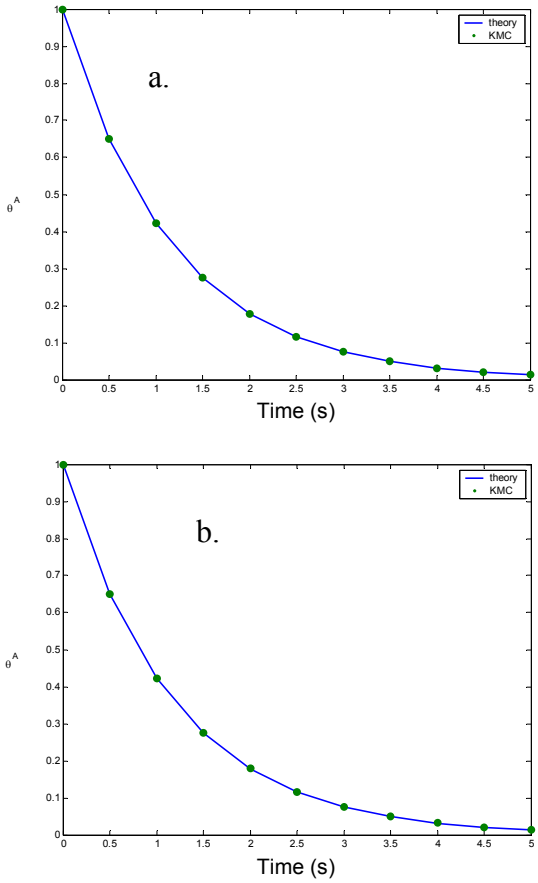

FIGURE 4. Fractional coverage of A versus time plots for 5.0 s **(a)** on a 10 μm × 10 μm surface with a 100 × 100 site simulation domain (100 nm mesoparticles) and **(b)** on a 2 μm × 2 μm surface with a 200 × 200 site simulation domain (10 nm mesoparticles). The theoretical coverage (the solid line) is computed from a standard first-order rate equation. Simulation results (the circles) are for a single seed number, since all seed numbers will give the same results.

$$J = -D\frac{\partial c}{\partial y} = D\frac{\left(c_1 - c_2\right)}{\Delta L}, \tag{6}$$

In terms of the jump frequencies to the diagonal and horizontal (= vertical) sites, the flux from plane 1 to plane 2 is

$$J = \left(c_1 - c_2\right)\left(2w_d + w_h\right)\Delta L \tag{7}$$

Combining Eqs. (6) and (7) gives the diffusion coefficient in terms of the jump frequencies:

$$D = \left(2w_d + w_h\right)\left(\Delta L\right)^2 \tag{8}$$

Taking the $\sqrt{2}$ difference in length scales from the diagonal and horizontal lattice sites into account gives $w_h = 2w_d$, which is substituted into Eq. (8) and solved to give

$$w_h = \frac{D}{2\left(\Delta L\right)^2} \tag{9}$$

$$w_d = \frac{D}{4\left(\Delta L\right)^2} \tag{10}$$

which is implemented in the KMC code. For realistic values of the physical parameters, the time increment [Eq. (2)] is dominated by the high-surface diffusion rate relative to the other reaction rates, so the inverse quadratic scaling of the rate [Eq. (5)] with the lattice spacing implies that the time increment increases with lattice spacing. Hence the computational cost of coarse-grained KMC simulation for a fixed surface area is reduced by increasing the lattice spacing both by the reduction of the number of lattice sites and by the increase in the time increment. These results are consistent with similar observations reported previously for other classes of coarse-grained KMC simulations [2].

The consistency of the surface diffusion implementation was verified by placing a single mesoparticle in the middle of a surface and allowing it to diffuse. A theoretical expression for 2D diffusion is [27, 28, 30]

$$< x^2 > = 4Dt, \tag{11}$$

where $\langle x^2 \rangle$ is the averaged squared distance from the initial position, D is the diffusion coefficient, and t is time. Comparing the slope of a line through $\langle x^2 \rangle$ data vs. time with the theoretical slope of 4D provides a metric to gauge whether or not surface diffusion is being simulated correctly in the KMC simulation code. In the trial calculations reported in Fig. 5, a 1000 × 1000 lattice was used so that the mesoparticle could travel relatively long distances for a relatively long time without crossing the periodic boundaries. To account for the variability in the data, maximum likelihood estimation [31] was applied to attain error estimates on the slopes. The maximum likelihood (ML) slope and 99% confidence intervals for the slope are

$$\text{ML slope} = 7.4 \times 10^{-10}\ \text{m}^2/\text{s} \tag{12}$$

$$5.8\times10^{-10}\ \text{m}^2/\text{s} \le \text{slope} \le 9.0\times10^{-10}\ \text{m}^2/\text{s}. \tag{13}$$

The diffusion coefficient in the KMC code was 2.0×10^{-10} m^2/s, so $4D = 8.0\times10^{-10}$ m^2/s, which falls well within the confidence intervals for the simulations.

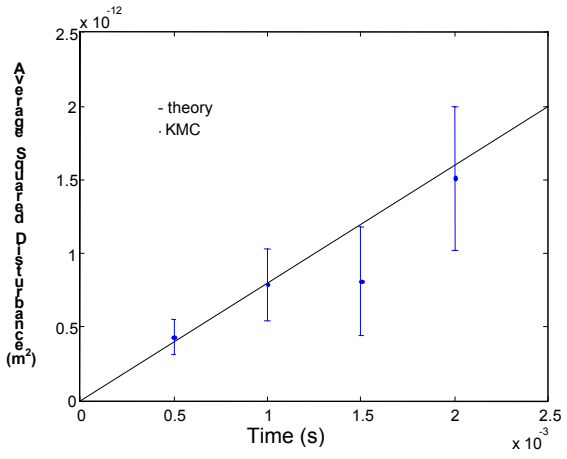

FIGURE 5. Average squared distance a single 25 nm mesoparticle traveled on a 1000 × 1000 2D grid for various times. Each point on the plots represents the average of 20 simulations with unique seed numbers. The 20 seed numbers used to generate each point were different for each point in order to eliminate time correlations.

3.3. Surface Reaction Second Order in Adsorbed Species

Several higher order surface reactions have been implemented in the KMC simulation code. Here it is shown how the reaction $2A(ads) + B(aq) \rightarrow 2C(ads)$ is implemented and verified. The reaction rate is

$$r_A^{'} = kC_A^{'2}\, C_B\big|_{z=0} \tag{14}$$

where $C_A^{'}$ is the surface concentration of Species A, $C_B\big|_{z=0}$ is the concentration of Species B in the solution at the surface, and the rate constant k has units of m^5/mol^2-s. An accounting for the A-A pairs on the surface for both maximum and intermediate coverages gives the rate in the KMC code:

$$\text{rate}_{\text{MC}} = \frac{k\, C_B\big|_{z=0}}{8 N_A D_A^2}, \tag{15}$$

where N_A is Avagadro's number and D_A is the diameter of Species A.

Simulation results to verify the reaction implementation are reported in Fig. 6 for atomic and coarse-grained KMC simulations. At longer times, the KMC coverage of Species A begins to diverge from the theoretical coverage for a homogeneous surface (i.e., uniform surface concentrations), with the KMC coverage being lower. When the simulations are run to longer times, the KMC coverage of A becomes higher than the theoretical coverage and eventually remains constant at some nonzero value, because individual A mesoparticles become isolated from one another and thus remain unreacted. The deviation between the KMC results and the theoretical results, which assumes perfect mixing on the surface, diverge as the sur-

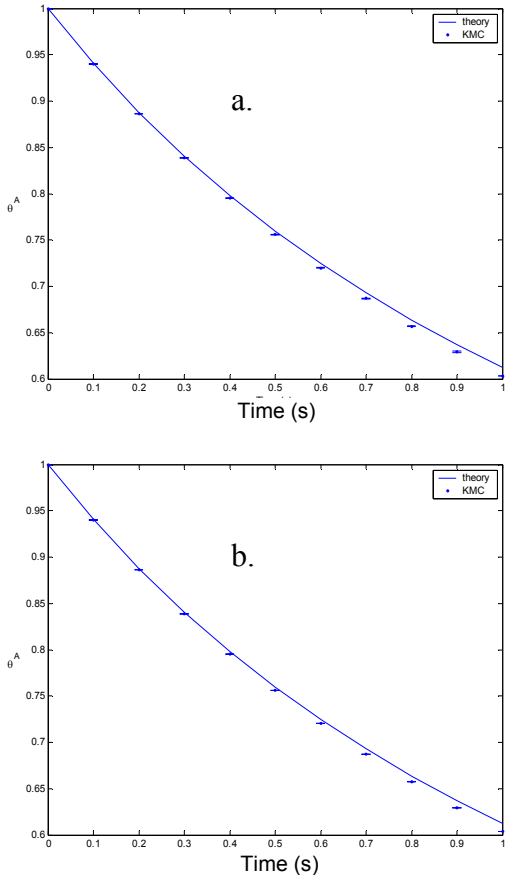

FIGURE 6. Comparison of theoretical and KMC-simulated coverage of species A as a function of time for the second-order reaction 2A(ads) + B(aq) → 2C(ads) for **(a)** atomic (0.256 nm) mesoparticles and a 100 × 100 domain and **(b)** 10 nm mesoparticles and a 200 × 200 domain. The initial fractional coverage of species A is 1.

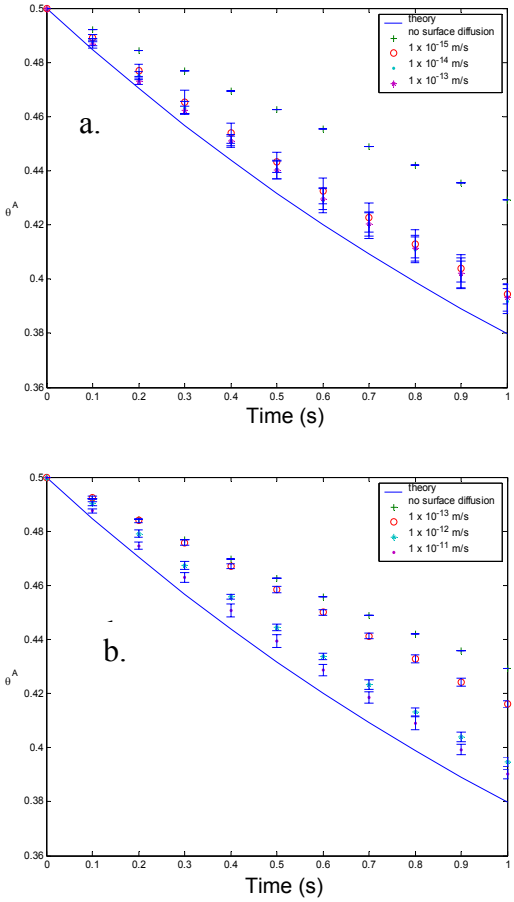

FIGURE 7. Comparison of theoretical and KMC-simulated coverage of species A as a function of time for the second-order reaction 2A(ads) + B(aq) → 2C(ads) for **(a)** atomic (0.256 nm) mesoparticles and a 100 × 100 domain and **(b)** 10 nm mesoparticles and a 200 × 200 domain. The initial fractional coverage of species A is 0.5. The KMC simulations had no species surface diffusing or species A surface diffusing at various rates.

face concentration of Species *A* decreases and surface diffusion becomes the limiting factor.

To investigate the role of surface diffusion, two series of simulations were carried out. In the first, only Species *A* was allowed to diffuse (see Fig. 7) and in the second both Species *A* and *C* were allowed to diffuse. In both cases, the mesoparticles were allowed to diffuse only on top of the surface, but not allowed over other mesoparticles of Species *A* or *C*. In both cases, simulations were started with an initial coverage of $\theta_A = 0.5$ so that the mesoparticles had places to diffuse on the surface. In addition, the initial configuration for the mesoparticles of Species *A* was that they were evenly dispersed across the surface. Simulation results with surface diffusion of Species *A* are shown in Fig. 7 and with surface diffusion of both Species *A* and *C* are shown in Fig. 8. In both figures, the simulated coverage of *A* is higher than the theoretical coverage for a homogeneous surface for all times; moreover, the deviation increases with time. With an increase in the surface diffusion coefficient of Species *A*, the conversion of

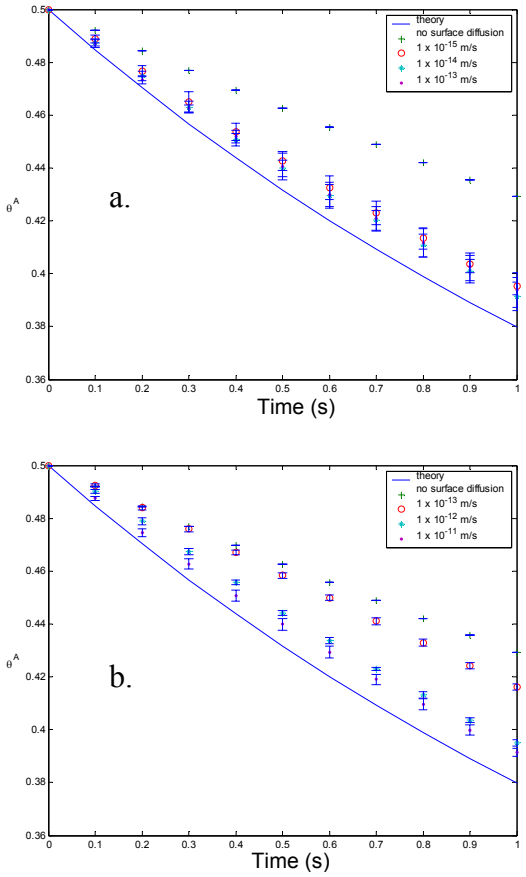

FIGURE 8. Comparison of theoretical and KMC-simulated coverage of species A as a function of time for the second-order reaction 2A(ads) + B(aq) → 2C(ads) for **(a)** atomic (0.256 nm) mesoparticles and a 100 × 100 domain and **(b)** 10 nm mesoparticles and a 200 × 200 domain. The initial fractional coverage of species A is 0.5. The KMC simulations had no species surface diffusing or species A and C surface diffusing at various rates.

Species *A* simulated by the KMC code approaches the theoretical coverage for a homogeneous surface of *A* as a function of time.

Higher values of the surface diffusion coefficient required additional computational time for a given level of coarse-graining. To have the KMC model exactly match the theoretical results, the surface diffusion coefficient would have to be increased substantially, which would be computationally infeasible. It may be recognized that, for the same values of the diffusion coefficients, the KMC results are nearly the same whether *C* is allowed to diffuse or not, which suggests that the surface composition is similar in either case.

4. SIMULATIONS FOR AN ELECTRO CHEMICAL/CHEMICAL MECHANISM

A set of reaction steps that is typically found in additive mechanisms associated with electrodeposition was simulated with the KMC simulation code, and results were compared to the theoretical coverage of the additive species calculated from kinetic expressions by assuming a homogeneous surface. The mechanism that was chosen for illustration here was

1. $A(aq) + e^- \rightarrow B(ads)$
2. $B(ads) \rightarrow A(aq) + e^-$
3. Surface diffusion of *B*
4. $B(ads) + e^- \rightarrow C(s)$
5. $C(s) \rightarrow B(ads) + e^-$
6. $2B(ads) + D(aq) \rightarrow 2F(ads)$
7. $2F(ads) \rightarrow 2B(ads) + D(aq)$
8. Surface diffusion of *F*

Species *A* is only allowed to adsorb onto the substrate or onto Species *C*, but not onto Species *B* or *F*. Species *B* and *F* are allowed to diffuse over the electrode substrate or over Species C, but not over Species *B* or Species *F* because those moves could lead to nonphysical results. The parameters associated with the actions in the mechanism are listed in Table 1.

The simulation results are shown in Fig. 9 for the atomic-scale and Fig. 10 for the mesoscale. In Fig. 9a, the KMC simulations do not have any surface diffusion of Species *B* or *F* and, as a result, the coverage of those species in the KMC simulations deviates significantly from the theoretical coverage for a homogenous surface, for most times. As the surface diffusion of Species *B* and *F* is increased to increase homogeneity at the surface in Figs. 9b–9d, the coverage's simulated by the KMC code approach the

TABLE 1. Physiochemical parameters used in the KMC simulations of a complex electrodeposition mechanism.

Reaction	Parameter	Value
$A(aq) + e^- \rightarrow B(ads)$	k	3×10^{-2} m^3/mol-s
$A(aq) + e^- \rightarrow B(ads)$	α	0.5
$B(ads) \rightarrow A(aq) + e^-$	k	5×10^{-2} 1/s
$B(ads) \rightarrow A(aq) + e^-$	α	0.5
$B(ads) + e^- \rightarrow C(s)$	k	5×10^{-2} 1/s
$B(ads) + e^- \rightarrow C(s)$	α	0.5
$C(s) \rightarrow B(ads) + e^-$	k	5×10^{-1} 1/s
$C(s) \rightarrow B(ads) + e^-$	α	0.5
$2B(ads) + D(aq) \rightarrow 2F(ads)$	k	5×10^{5} m^5/mol^2-s
$2F(ads) \rightarrow 2B(ads) + D(aq)$	k	5×10^{-7} m^2/mol-s

theoretical values. The simulation results in Fig. 10 follow trends that are similar to those shown in Fig. 9. As surface mixing is facilitated by increased surface diffusion, the coarse-grained KMC simulation results approach the theoretical predictions for a homogeneous surface.

5. CONCLUSIONS

A coarse-grained (2+1)D KMC simulation code was developed to address applications where a surface undergoes roughness evolution during electrodeposition in the presence of trace quantities of additives. The time required for the test calculations increased superlinearly with the number of lattice sites (Fig. 1). By comparing simulated results with various analytical results obtained from limiting cases of behavior, the validity of the KMC code was tested. It was found that the mass of copper deposited according to KMC simulations was with 1% of the theoretical value determined by Faraday's Law (Fig. 2) for lattices above 32 × 32. It was found that the surface roughness at a specified length scale can be accurately simulated by using a coarse-grained KMC code with lattice spacing of 1/10 or smaller of that length scale (Fig. 3). KMC simulations of fractional coverage of a species undergoing first-order reaction on the surface were found to be in close agreement with theoretical values obtained analytically for 10 and 100 nm mesoparticles for times up to 5 s investigated here (Fig. 4). Diffusion of a single mesoparticle on a planar 2D surface was found to obey the analytical expression to well within the 95% confidence level for both 25 and 100 nm mesoparticles (Fig. 5).

For second-order homogeneous surface reactions, it is shown that the KMC simulated surface coverage approaches the analytical surface coverage as surface mixing is increased by increasing the surface diffusion rate. When surface diffusion of reacting species was included in the KMC simulations, it was found to be computationally expensive to increase the diffusion coefficient to sufficiently large values to achieve close agreement with analytical results obtained with the assumption of rapid diffusion (Figs. 7 and 8). Simulations involving large values of surface diffusion coefficients were found to be more computationally efficient when using coarse-graining. For a typical multistep additive mechanism involving surface diffusion, it was found that the time variation of surface coverage of reaction intermediates obtained analytically was in agreement to within 10% for both atomic-scale KMC simulations (Fig. 9) and 10 nm mesoparticles

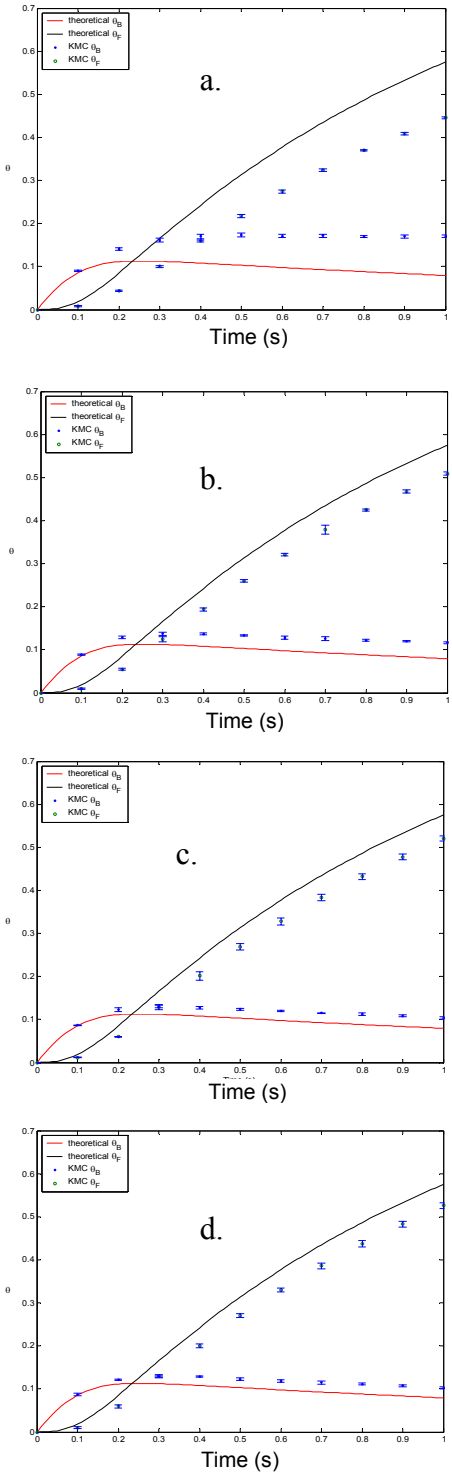

FIGURE 9. Comparison of theoretical and KMC simulated coverage of species B and F as a function of time for the complex reaction mechanism for atomic (0.256 nm) mesoparticles and a 100 × 100 domain. The KMC simulations had species B and F surface diffusing. The simulations had surface diffusion rate constants of species B and F of **(a)** 0 m/s, **(b)** 1×10^{-14} m/s, **(c)** 1×10^{-13} m/s, and **(d)**1×10^{-12} m/s.

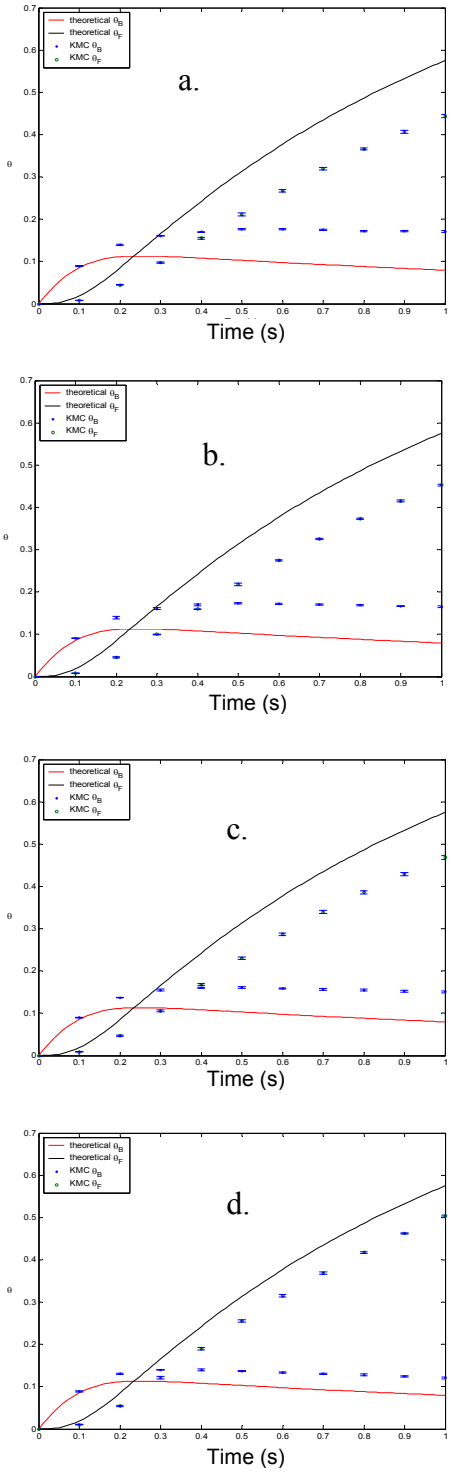

FIGURE 10. Comparison of theoretical and KMC-simulated coverage of species B and F as a function of time for the complex reaction mechanism for 10 nm mesoparticles and a 200 × 200 domain. The KMC simulations had species B and F surface diffusing. The simulations had surface diffusion rate constants of species B and F of **(a)** 0 m/s, **(b)** 1×10^{-13} m/s, **(c)** 1×10^{-12} m/s, and **(d)**. 1×10^{-11} m/s.

(Fig. 10). The results verified the numerical accuracy and the reduced computational cost of the coarse-grained KMC approach for simulating complex chemical and electrochemical mechanisms.

ACKNOWLEDGMENTS

Funding for this work was provided by an IBM Faculty Partnership and the National Science Foundation under Grants ACI 96-19019, CTS-0135621, and NSF PACI NRAC MCA-01S022. Any opinions, findings, and conclusions or recommendations expressed in this material are those of the authors and do not necessarily reflect the views of the National Science Foundation. The first author received funding from the H. G. Drickamer Fellowship from the Department of Chemical and Biomolecular Engineering at the University of Illinois.

REFERENCES

1. Katsoulakis, M. A., Majda, A. J., and Vlachos, D. G. Coarse-grained stochastic processes and Monte Carlo simulations in lattice systems, *J. Comp. Phys.* **186**:250–278, 2003.
2. Katsoulakis, M. A., and Vlachos, D. G. Coarse-grained stochastic processes and kinetic Monte Carlo Simulatore for the diffusion of interacting particles, J. Chem. Phys. **119**:9412–9427, 2003.
3. Shelley, J. C., and Shelley, M. Y. Computer simulation of surfactant solutions, *Cur. Opin. in Col. and Surf. Sci.* **5**:101–110, 2000.
4. Jönsson, M, Skepö, M., Tjerneld, F., and Linse, P. Effect of spatially distributed surface residues on protein-polymer association, *J. Phys. Chem.* B **107**:5511–5518, 2003.
5. Lopez, C. F., Moore, P. B., Shelley, J. C., Shelley, M. Y., and Klein, M. L. Computer simulation studies of biomembranes using a coarse grain model, *Comp. Phys. Comm.* **147**:1–6, 2002.
6. Ismail, A. E., Rutledge, G. C., and Stephanopoulos, G. Multiresolution analysis in statistical mechanics: I. Using wavelets to calculate thermodynamic properties, *J. Chem. Phys.* **118**:4414–4423, 2003.
7. Pricer, T. J., Kushner, M. J., and Alkire, R. C. Monte Carlo simulation of the electrodeposition of copper: I. Additive-free acidic sulfate solution, *J. Electrochem. Soc.* **149**:C396–C405, 2002.
8. Pricer, T. J., Kushner, M. J., and Alkire, R. C. Monte Carlo simulation of the electrodeposition of copper: II. Acid sulfate solution with blocking additive, *J. Electrochem. Soc*. **149**:C406–C412, 2002.
9. Drews, T. O., Ganley, J. C., and Alkire, R. C. Evolution of surface roughness during copper electrodeposition in the presence of additives: Comparison of experiments and Monte Carlo simulations, *J. Electrochem. Soc.* **150**:C325–C334, 2003.
10. Drews, T. O., Webb, E. G., Ma, D. L., Alameda, J., Braatz, R. D., and Alkire, R. C. Coupled mesoscale-continuum simulations of copper electrodeposition in a trench, *AIChE J.* **50**:226-240, 2004.
11. Drews, T. O., Braatz, R. D., and Alkire, R. C. Parameter sensitivity analysis of Monte Carlo simulations of copper electrodeposition in the presence of multiple additives, *J. Electrochem. Soc.* **150**:C807–C812, 2003**.**
12. Dooling, D. J., and Broadbelt, L. J. Generic Monte Carlo tool for kinetic modeling, *Ind. Eng. Chem. Res.* 40:522–529, 2001.
13. Pal, S., and Landau, D. P. Monte Carlo simulation and dynamic scaling of surfaces in MBE growth, *Phys. Rev. B* **49**:10597–10606, 1994.
14. Kalke, M., and Baxter, D. V. A kinetic Monte Carlo simulation of chemical vapor deposition: Non-monotonic variation of surface roughness with growth temperature, *Surf. Sci.* **477**:95–101, 2001.

15. Larsson, M. I., Ni, W.-X., and Hansson, G. V. Manipulation of nucleation by growth rate modulation, *J. Appl. Phys.* **78**:3792–3796, 1995.

16. Fichthorn, K. A., and Weinberg, W. H. Theoretical foundations of dynamical Monte Carlo simulations, *J. Chem. Phys.* **95**:1090–1096, 1991.

17. Yang, Y. G., Johnson, R. A., and Wadley, H. N. G. Kinetic Monte Carlo simulation of heterometal epitaxial deposition, *Surf. Sci.* **499**:141–151, 2002.

18. Henkelman, G., and Jónsson, H. Long time scale kinetic Monte Carlo simulations without lattice approximation and predefined event table, *J. Chem. Phys.* **115**:9657–9666, 2001.

19. Levi, A. C., and Kotrla, M. Theory and simulation of crystal growth. J. Phys. Condens. Matter. 9: 299–344, 1994.

20. Battaile, C. C., Srolovitz, D. J., and Butler, J. E. A Kinetic Monte Carlo method for the atomic-scale simulation of chemical vapor deposition: application to diamond, *J. Appl. Phys.* **82**:6293–6300, 1997.

21. Lu, J., and Kushner, M. J. Trench filling by ionized metal physical vapor deposition, *J. Vac. Sci. Technol. A* **19**:2652–2663, 2001.

22. Bird, G.A., *Molecular Gas Dynamics and the Direct Simulation of Gas Flows*, Clarendon Press, Oxford, 1994.

23. Birdsall C. K., and Langdon, A.B., *Plasma Physics via Computer Simulation*, McGraw-Hill, New York, 1985.

24. Hebert, K. R. Analysis of current-potential hysteresis during electrodeposition of copper with additives *J. Electrochem. Soc.* **148**:C726–C732, 2001.

25. Kelly, J. J. and West, A. C. Copper deposition in the presence of polyethylene glycol: II. Electrochemical impedance spectroscopy, *J. Electrochem. Soc.* **145**:3477–3481, 1998.

26. Bard, A. J., and Faulkner, L. R., *Electrochemical Methods*, John Wiley & Sons, New York, 1980.

27. Voter, A. F. Classically exact overlayer dynamics: Diffusion of Rhodium clusters on Rh(100), *Phys. Rev. B* **34**:6819–6829, 1986.

28. Ala-Nissila, T., Ferrando, R., and Ying, S. C. Collective and single particle diffusion on surfaces. Adv. in Phys. 51:949–1078, 2002.

29. Kawamura, T., Kobayashi, A., and Das Sarma, S. Stochastic Simulation of Molecular-Beam Epitaxial Growth of a Model Compound Semiconductor: Effects of Kinetics, *Phys. Rev. B*. **39:**12723–12734, 1989.

30. Shewmon, P. G., *Diffusion in Soli*ds, McGraw-Hill, New York, 1963.

31. Chung, S. H., Ma, D. L., and Braatz, R. D., Optimal model-based experimental design in batch crystallization, *Chem. and Intel. Lab. Syst.* **50**:83–90, 2000.